Inorganic Chemistry

pubs.acs.org/IC

Communication

Copper(II) Binding to the Intrinsically Disordered C-Terminal Peptide of SARS-CoV-2 Virulence Factor Nsp1

Maryann Morales, Raheleh Ravanfar, Paul H. Oyala, Harry B. Gray,* and Jay R. Winkler*

Cite This: *Inorg. Chem.* 2022, 61, 8992−8996

Read Online

ACCESS | Metrics & More | Article Recommendations | Supporting Information

ABSTRACT: The first encoded SARS-CoV-2 protein (Nsp1) binds to the human 40S ribosome and blocks synthesis of host proteins, thereby inhibiting critical elements of the innate immune response. The final 33 residues of the natively unstructured Nsp1 C-terminus adopt a helix-turn-helix geometry upon binding to the ribosome. We have characterized the fluctuating conformations of this peptide using circular dichroism spectroscopy along with measurements of tryptophan fluorescence and energy transfer. Tryptophan fluorescence decay kinetics reveal that copper(II) binds to the peptide at micromolar concentrations, and electron paramagnetic resonance spectroscopy indicates that the metal ion coordinates to the lone histidine residue.

The human innate immune system is the first line of defense against invading pathogens. For viral pathogens, the type I interferon (IFN-I) response is an integral element of this primary protection mechanism.[1] In their battle for survival, viruses evolve mechanisms to evade the host immune response. The SARS-CoV and SARS-CoV-2 viruses inhibit the IFN-I response, giving the virus time to replicate before being assaulted by the immune system. These viruses deploy a multipronged attack on IFN-I involving several viral proteins.[1,2]

The SARS-CoV-2 viral genome is positive-sense single-stranded mRNA coding for 29 proteins in 14 open reading frames (ORFs).[3] ORF1ab encodes a polyprotein that is autoproteolyzed into 16 nonstructural proteins (Nsp1−Nsp16). The first protein in the SARS-CoV and SARS-CoV-2 polyprotein sequence (Nsp1) has been shown to inhibit IFN-I response through several different mechanisms,[4] including inhibition of host mRNA nuclear export,[5] degradation of host mRNA,[6] and inhibition of protein translation.[7,8] A key element of Nsp1 protein translation inhibition involves binding to the 40S ribosome,[9,10] and importantly, recent cryo-EM studies have provided structural insights into the Nsp1−40S interaction.[11−13] The 180-residue SARS-CoV-2 Nsp1 protein contains a well-structured N-terminal globular domain (residues 11−125) and an unstructured C-terminal tail.[14] Upon binding to the 40S ribosome, Nsp1 residues 148−180 adopt a helix-turn-helix structure that blocks the mRNA entry tunnel (Figure 1).[11,12] Nsp1 at a concentration of 1 μM inhibited *in vitro* protein synthesis by 90% or more.[12] This would be a suicidal interaction for the virus were it not for the fact that Nsp1 binding to the ribosome inhibits host protein translation to a greater extent than viral protein translation due to the unique 5′ untranslated region of viral mRNA.[7]

Nsp1 is a potent SARS-Cov-2 virulence factor and is an obvious antiviral drug target. The absence of folded structure in the C-terminal Nsp1 polypeptide rules out structure-based drug discovery approaches. Intrinsically disordered proteins (IDPs) and intrinsically disordered protein regions (IDPRs)

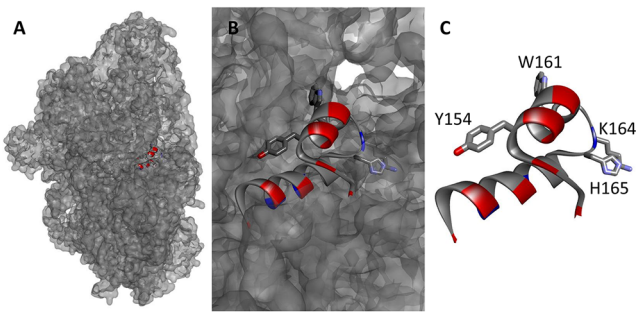

Figure 1. (A) Structural model of Nsp1-CT bound to the human 40S ribosomal subunit (PDB ID 6ZOK). (B) Magnified view illustrating the side chains of Y154, W161, K164, and H165. (C) Ribbon diagram of Nsp1-CT highlighting the positions of the four amino acids.

are common in viral proteomes and may be one reason for their success.[15] Flexible protein regions confer plasticity and adaptability that enable viruses to survive in unpredictable and hostile environments. IDPs and IDPRs develop structure upon binding to host targets, but these low-affinity, high-specificity interactions are difficult to inhibit by using conventional therapeutic strategies because of the absence of static ligand pockets.

Transition metals are attractive candidates for SARS-CoV-2 Nsp1 inhibitors because of the presence of several potential ligands among residues 148−180 (Ac-ELGTDPYED-FQENWNTKHSSGVTRELMRELNGG). Among the dipositive first-row transition metal ion candidates for binding to H165, we picked Cu(II) for initial study, as it has the greatest

Received: April 19, 2022
Published: June 6, 2022

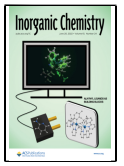

https://doi.org/10.1021/acs.inorgchem.2c01329
Inorg. Chem. 2022, 61, 8992−8996

affinity for imidazole.[16] In addition, Cu(II) is known to bind to unstructured peptides, often with additional coordination of deprotonated amide nitrogen atoms from nearby residues.[17−21] What is more, studies of the prion protein indicate that unstructured octarepeats (PHGGGWGQ) bind Cu(II) preferentially over several other dipositive metal cations.[22] Employing laser spectroscopy, including time-resolved fluorescence energy transfer (TR-FRET), we have obtained nanosecond snapshots of rapidly fluctuating conformations in the Nsp1 C-terminal peptide (Nsp1-CT). Importantly, we have shown that these conformations are altered by copper(II) binding, which could prevent Nsp1 from blocking immune responses. We suggest that our work will aid designs of inorganic agents for COVID-19 therapy.

The far-UV circular dichroism (CD) spectrum of Nsp1-CT features a negative ellipticity minimum at 200 nm and a negative ellipticity shoulder near 230 nm (Figure S1). The molar ellipticity minimum at 200 nm is about 40% of that expected for a random coil, suggesting an offsetting positive contribution from β-sheet or turn structures.[23] Decomposition of the spectrum into three components (α-helix, β-sheet, and random coil) indicates that the peptide adopts a dominant random coil configuration with an admixture of β-sheet and minimal (<5%) α-helix.[23]

Tryptophan fluorescence reports on the polarity of the environment around the indole chromophore.[24] The Nsp1-CT W161 fluorescence maximizes at 350 nm, consistent with a solvent-exposed indole group. As expected for tryptophan incorporated into a polypeptide, a multiexponential function is required to model the indole fluorescence decay kinetics (Table S1).

$$\langle\tau\rangle = \int_0^\infty \frac{I(t) - I(\infty)}{I(0) - I(\infty)}\,dt \tag{1}$$

The W161 effective fluorescence decay time (eq 1) is about 2.4(2) ns, somewhat shorter than that of W4 in α-synuclein ($\langle\tau\rangle \approx 2.9$ ns),[25] for example. The shorter lifetime suggests the presence of an additional quenching pathway for the singlet excited indole in Nsp1-CT W161.

Tryptophan and 3-nitrotyrosine (YNO_2) constitute a fluorescence energy-transfer pair with a Förster distance of 26 Å.[26] Introduction of YNO_2 at position 154 in Nsp1-CT reduces the W161 effective fluorescence decay time to about 1 ns (Figure 2). In the cryoEM structure of Nsp1 bound to the 40S ribosomal subunit, the centroid-to-centroid distance between W161 and Y154 is 15.4 Å. The W161−Y154 distance in a β-sheet model of Nsp1-CT is 29.7 Å. The simplest application of the Förster[27] energy-transfer model for the *W161 decay in Nsp1-CT-Y(NO_2)154 using effective decay times suggests a W161−Y(NO_2)154 distance of 24 Å. Because Nsp1-CT is a disordered polypeptide, a distribution of W161−Y(NO_2)154 distances likely would be required to describe the *W161 decay. We extracted a minimum-entropy, model-independent distribution of W161−Y(NO_2)154 distances from the energy-transfer kinetics (Figure 2). Three populations of W161−Y(NO_2)154 distances describe the energy-transfer kinetics: ∼13 Å (29%), ∼17 Å (46%), and ∼28 Å (25%) The Nsp1-CT peptide appears to have a sizable fraction of extended structures between W161 and Y(NO_2)154, consistent with indications of β-sheet structure in the CD spectra.

At pH 6.5, Nsp1-CT has several residues with ligands available for binding to metal ions (eight carboxylates, one imidazole). Nsp1-CT W161 fluorescence is sensitive to low concentrations of Cu(II). At 30 μM peptide concentration, addition of 1 mol equiv of aquo Cu(II) leads to an ∼25% reduction in W161 fluorescence intensity. Cu(II) also produces a systematic reduction in the effective W161 fluorescence lifetime. Treating the reduction in $\langle\tau\rangle$ with a single Cu-binding-site model leads to a dissociation constant of 9.7 μM (pH 6.5) (Figure 3). *W161 fluorescence in an Nsp1 variant in which H165 is replaced by alanine (Nsp1-CT(H165A)) is only weakly quenched by Cu(II) with an apparent dissociation constant of 106 μM (Figure S2). This result is consistent with the relative Cu(II) binding constants of imidazole ($10^{4.02}$ M^{-1}) and a carboxylate (acetate, $10^{1.82}$ M^{-1}).[16] Importantly, the *W161 quenching data clearly implicate H165 as the site of Cu(II) coordination to Nsp1-CT.

Aquo Cu(II) likely quenches *W161 by electron transfer (ET). The decrease in effective lifetime is consistent with a quenching rate constant of 5×10^8 s^{-1}. A driving-force

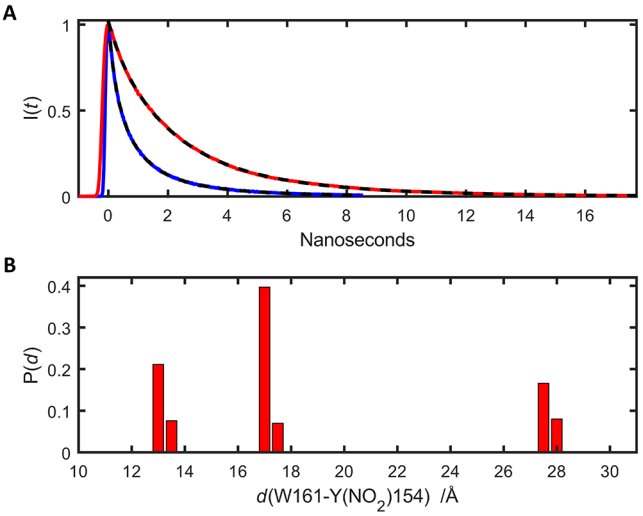

Figure 2. (A) Nsp1-CT (red) and Nsp1-CT-Y(NO_2)154 (blue) W161 fluorescence decay kinetics ([Nsp1-CT] = 30 μM, pH 6.5, MOPS 20 mM). Dashed black lines are fits to multiexponential decay functions with $\langle\tau\rangle$ values of 2.4 and 0.9 ns. (B) Probability distribution of W161−Y(NO_2)154 distances extracted from W161 energy transfer kinetics.

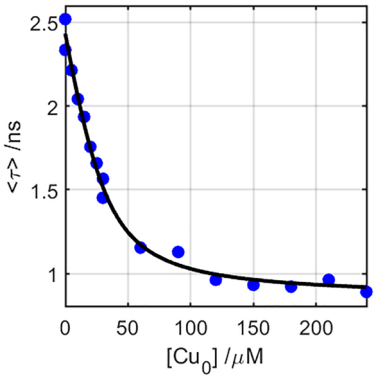

Figure 3. Variation in Nsp1-CT W161 effective fluorescence decay time ($\langle\tau\rangle$) as a function of Cu(II) concentration. Solid line is a fit to a single binding site model with K_d = 9.7 μM ([Nsp1-CT] = 30 μM, pH 6.5, MOPS 20 mM, 30% glycerol).

https://doi.org/10.1021/acs.inorgchem.2c01329
Inorg. Chem. 2022, 61, 8992−8996

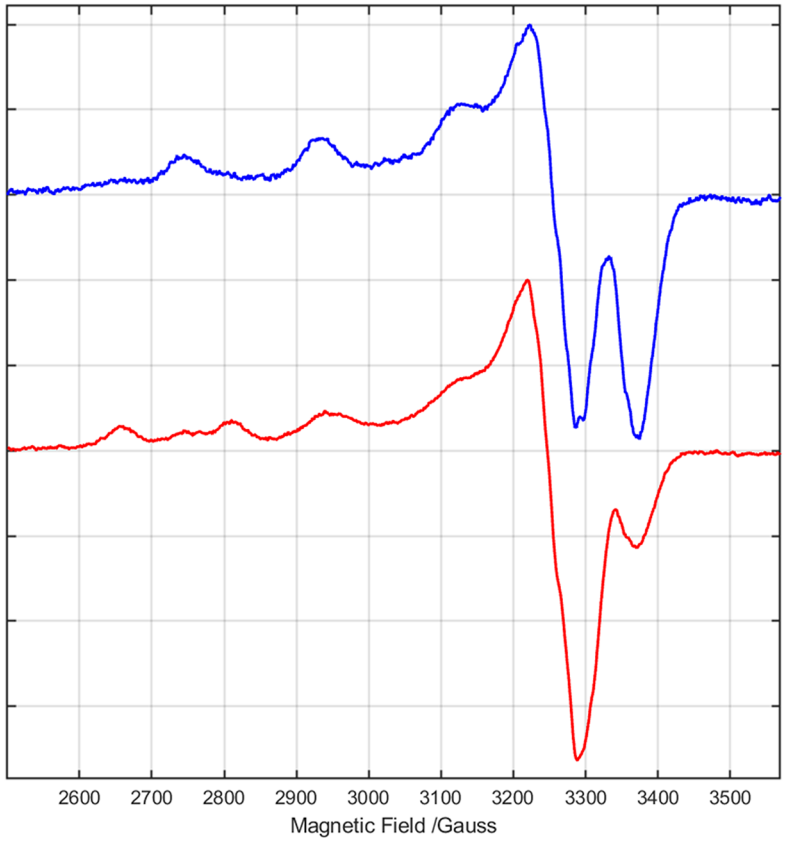

Figure 4. X-band EPR spectra of Cu(II):Nsp1-CT ([Cu] = [Nsp1-CT] = 100 μM, MOPS 20 mM, 30% glycerol) at pH 6.5 (red) and 7.5 (blue).

optimized ET rate constant of this magnitude in a folded protein would imply a donor−acceptor distance of 10−14 Å.[28] This range is compatible with the 14 Å distance from the W161 indole to Nε of H165 in the helix-turn-helix structure of Nsp1 bound to the 40S ribosome.[11−13] But, as the far-UV CD spectrum does not indicate that substantial α-helical structure develops when Cu(II) is added to Nsp1-CT (Figure S1), it is likely that Cu(II):Nsp1-CT adopts a different conformation in solution.

An alternative interpretation of the quenching W161 rate constant is that it reflects the specific rate of intrachain diffusion that brings the Cu(II)-bound residue in contact with *W161. The rate constant for quenching by the peptide-bound Cu(II) complex ($\sim 5 \times 10^8$ s^{-1}) is at least an order of magnitude greater than the fastest tertiary contact formation observed for disordered polypeptides.[29−32]

Electron paramagnetic resonance (EPR) spectroscopy is a sensitive probe of the Cu(II) coordination environment. The continuous wave X-band spectrum of Nsp1-CT (100 μM) in the presence of 1 equiv of Cu(II) at pH 6.5 (Figure 4) indicates a dominant species with near-axial Cu(II) coordination (g_1 = 2.060, g_2 = 2.058, g_3 = 2.332) (Figure S3). The hyperfine coupling constant for the low-field resonance (g_3) is A_3 = 457 MHz. The spectrum provided no evidence for residual aquo Cu(II) (Figure S5), indicating that Cu(II) binds to a single Nsp1-CT peptide under these conditions. Comparison of the EPR parameters to the Peisach−Blumberg[33] $g_{\|}$−$A_{\|}$ correlation suggests Cu(II) coordination to one nitrogen and three oxygen atoms.

At pH 7.5 the Cu(II) paramagnetic resonance spectrum is more rhombic, and the g-values are shifted to higher magnetic fields (g_1 = 2.040, g_2 = 2.067, g_3 = 2.219; A_3 = 583 MHz), indicating a less symmetric but stronger ligand field around Cu(II) (Figure 4 and Figure S4). The EPR spectrum of aquo Cu(II) in the presence of Nsp1-CT(H165A) at pH 7.5 was little changed from that of Cu(II) in buffer. The Peisach−Blumberg correlation indicates 3N, 1O coordination to Cu(II) at this pH.[33] Cu(II) binding to His residues in peptides is typically accompanied by coordination of deprotonated amide nitrogens from one or two C-terminal residues after His. The EPR parameters in these systems are closely analogous to those of Cu:Nsp1-CT.[17−20] The stronger ligand field implied by the reduced g-values at pH 7.5 is consistent with Nsp1 N-amide coordination to Cu(II).

Experience with the SARS-CoV-2 pandemic has demonstrated that multiple strategies are required to protect populations from this virus. Of the 29 proteins encoded in the SARS-CoV-2 genome, the Nsp1 virulence factor is an attractive target for antiviral treatments. Competitive inhibition of Nsp1 binding to the 40S ribosome could relieve some of the immune suppression that helps this virus survive and multiply. The absence of stable secondary and tertiary structure in the ribosome-binding region of Nsp1 renders structure-based drug design ineffective. Our measurements have demonstrated that Cu(II) binds with micromolar affinity to the Nsp1-CT peptide, likely involving coordination to H165. Of course, aquo Cu(II) is not a practical *in vivo* inhibitor, but strategies that combine H165-metal coordination with binding to nearby regions of the Nsp1 peptide might be a promising approach to the development of inhibitors to this source of SARS-CoV-2 virulence.

https://doi.org/10.1021/acs.inorgchem.2c01329
Inorg. Chem. 2022, 61, 8992−8996

■ ASSOCIATED CONTENT

Supporting Information

The Supporting Information is available free of charge at https://pubs.acs.org/doi/10.1021/acs.inorgchem.2c01329.

Detailed experimental procedures, table of tryptophan fluorescence decay kinetics parameters, UV CD spectra, simulations of X-band EPR data (Figures S1−S5, Table S1) (PDF)

■ AUTHOR INFORMATION

Corresponding Authors

Harry B. Gray − *Beckman Institute, California Institute of Technology, Pasadena, California 91125, United States;* orcid.org/0000-0002-7937-7876; Email: hbgray@caltech.edu

Jay R. Winkler − *Beckman Institute, California Institute of Technology, Pasadena, California 91125, United States;* orcid.org/0000-0002-4453-9716; Email: winklerj@caltech.edu

Authors

Maryann Morales − *Beckman Institute, California Institute of Technology, Pasadena, California 91125, United States*

Raheleh Ravanfar − *Beckman Institute, California Institute of Technology, Pasadena, California 91125, United States*

Paul H. Oyala − *Beckman Institute, California Institute of Technology, Pasadena, California 91125, United States;* orcid.org/0000-0002-8761-4667

Complete contact information is available at: https://pubs.acs.org/10.1021/acs.inorgchem.2c01329

Funding

The work was supported by the Arnold and Mabel Beckman Foundation and by the National Institute of Diabetes and Digestive and Kidney Diseases of the National Institutes of Health under Award R01DK019038. The content is solely the responsibility of the authors and does not necessarily represent the official views of the National Institutes of Health.

Notes

The authors declare no competing financial interest.

■ REFERENCES

(1) Lei, X.; Dong, X.; Ma, R.; Wang, W.; Xiao, X.; Tian, Z.; Wang, C.; Wang, Y.; Li, L.; Ren, L.; Guo, F.; Zhao, Z.; Zhou, Z.; Xiang, Z.; Wang, J. Activation and evasion of type I interferon responses by SARS-CoV-2. *Nat. Commun.* **2020**, *11* (1), 3810.

(2) Bouayad, A. Innate immune evasion by SARS-CoV-2: Comparison with SARS-CoV. *Reviews in Medical Virology* **2020**, *30* (6), e2135.

(3) Gordon, D. E.; Jang, G. M.; Bouhaddou, M.; Xu, J.; Obernier, K.; White, K. M.; O'Meara, M. J.; Rezelj, V. V.; Guo, J. Z.; Swaney, D. L.; Tummino, T. A.; Hüttenhain, R.; Kaake, R. M.; Richards, A. L.; Tutuncuoglu, B.; Foussard, H.; Batra, J.; Haas, K.; Modak, M.; Kim, M.; Haas, P.; Polacco, B. J.; Braberg, H.; Fabius, J. M.; Eckhardt, M.; Soucheray, M.; Bennett, M. J.; Cakir, M.; McGregor, M. J.; Li, Q.; Meyer, B.; Roesch, F.; Vallet, T.; Mac Kain, A.; Miorin, L.; Moreno, E.; Naing, Z. Z. C.; Zhou, Y.; Peng, S.; Shi, Y.; Zhang, Z.; Shen, W.; Kirby, I. T.; Melnyk, J. E.; Chorba, J. S.; Lou, K.; Dai, S. A.; Barrio-Hernandez, I.; Memon, D.; Hernandez-Armenta, C.; Lyu, J.; Mathy, C. J. P.; Perica, T.; Pilla, K. B.; Ganesan, S. J.; Saltzberg, D. J.; Rakesh, R.; Liu, X.; Rosenthal, S. B.; Calviello, L.; Venkataramanan, S.; Liboy-Lugo, J.; Lin, Y.; Huang, X.-P.; Liu, Y.; Wankowicz, S. A.; Bohn, M.; Safari, M.; Ugur, F. S.; Koh, C.; Savar, N. S.; Tran, Q. D.; Shengjuler, D.; Fletcher, S. J.; O'Neal, M. C.; Cai, Y.; Chang, J. C. J.; Broadhurst, D. J.; Klippsten, S.; Sharp, P. P.; Wenzell, N. A.; Kuzuoglu-Ozturk, D.; Wang, H.-Y.; Trenker, R.; Young, J. M.; Cavero, D. A.; Hiatt, J.; Roth, T. L.; Rathore, U.; Subramanian, A.; Noack, J.; Hubert, M.; Stroud, R. M.; Frankel, A. D.; Rosenberg, O. S.; Verba, K. A.; Agard, D. A.; Ott, M.; Emerman, M.; Jura, N.; von Zastrow, M.; Verdin, E.; Ashworth, A.; Schwartz, O.; d'Enfert, C.; Mukherjee, S.; Jacobson, M.; Malik, H. S.; Fujimori, D. G.; Ideker, T.; Craik, C. S.; Floor, S. N.; Fraser, J. S.; Gross, J. D.; Sali, A.; Roth, B. L.; Ruggero, D.; Taunton, J.; Kortemme, T.; Beltrao, P.; Vignuzzi, M.; García-Sastre, A.; Shokat, K. M.; Shoichet, B. K.; Krogan, N. J. A SARS-CoV-2 protein interaction map reveals targets for drug repurposing. *Nature* **2020**, *583* (7816), 459−468.

(4) Narayanan, K.; Huang, C.; Lokugamage, K.; Kamitani, W.; Ikegami, T.; Tseng, C.-T. K.; Makino, S. Severe Acute Respiratory Syndrome Coronavirus nsp1 Suppresses Host Gene Expression, Including That of Type I Interferon, in Infected Cells. *J. Virol.* **2008**, *82* (9), 4471−4479.

(5) Zhang, K.; Miorin, L.; Makio, T.; Dehghan, I.; Gao, S.; Xie, Y.; Zhong, H.; Esparza, M.; Kehrer, T.; Kumar, A.; Hobman, T. C.; Ptak, C.; Gao, B.; Minna, J. D.; Chen, Z.; García-Sastre, A.; Ren, Y.; Wozniak, R. W.; Fontoura, B. M. A. Nsp1 protein of SARS-CoV-2 disrupts the mRNA export machinery to inhibit host gene expression. *Science Advances* **2021**, *7* (6), eabe7386.

(6) Kamitani, W.; Narayanan, K.; Huang, C.; Lokugamage, K.; Ikegami, T.; Ito, N.; Kubo, H.; Makino, S. Severe acute respiratory syndrome coronavirus nsp1 protein suppresses host gene expression by promoting host mRNA degradation. *Proc. Natl. Acad. Sci. U. S. A.* **2006**, *103* (34), 12885−12890.

(7) Finkel, Y.; Gluck, A.; Nachshon, A.; Winkler, R.; Fisher, T.; Rozman, B.; Mizrahi, O.; Lubelsky, Y.; Zuckerman, B.; Slobodin, B.; Yahalom-Ronen, Y.; Tamir, H.; Ulitsky, I.; Israely, T.; Paran, N.; Schwartz, M.; Stern-Ginossar, N. SARS-CoV-2 uses a multipronged strategy to impede host protein synthesis. *Nature* **2021**, *594* (7862), 240−245.

(8) Lokugamage, K. G.; Narayanan, K.; Huang, C.; Makino, S. Severe Acute Respiratory Syndrome Coronavirus Protein nsp1 Is a Novel Eukaryotic Translation Inhibitor That Represses Multiple Steps of Translation Initiation. *J. Virol.* **2012**, *86* (24), 13598−13608.

(9) Kamitani, W.; Huang, C.; Narayanan, K.; Lokugamage, K. G.; Makino, S. A two-pronged strategy to suppress host protein synthesis by SARS coronavirus Nsp1 protein. *Nature Structural & Molecular Biology* **2009**, *16* (11), 1134−1140.

(10) Lapointe, C. P.; Grosely, R.; Johnson, A. G.; Wang, J.; Fernández, I. S.; Puglisi, J. D. Dynamic competition between SARS-CoV-2 NSP1 and mRNA on the human ribosome inhibits translation initiation. *Proc. Natl. Acad. Sci. U. S. A.* **2021**, *118* (6), e2017715118.

(11) Thoms, M.; Buschauer, R.; Ameismeier, M.; Koepke, L.; Denk, T.; Hirschenberger, M.; Kratzat, H.; Hayn, M.; Mackens-Kiani, T.; Cheng, J.; Straub, J. H.; Stürzel, C. M.; Fröhlich, T.; Berninghausen, O.; Becker, T.; Kirchhoff, F.; Sparrer, K. M. J.; Beckmann, R. Structural basis for translational shutdown and immune evasion by the Nsp1 protein of SARS-CoV-2. *Science* **2020**, *369* (6508), 1249−1255.

(12) Schubert, K.; Karousis, E. D.; Jomaa, A.; Scaiola, A.; Echeverria, B.; Gurzeler, L.-A.; Leibundgut, M.; Thiel, V.; Mühlemann, O.; Ban, N. SARS-CoV-2 Nsp1 binds the ribosomal mRNA channel to inhibit translation. *Nature Structural & Molecular Biology* **2020**, *27* (10), 959−966.

(13) Yuan, S.; Peng, L.; Park, J. J.; Hu, Y.; Devarkar, S. C.; Dong, M. B.; Shen, Q.; Wu, S.; Chen, S.; Lomakin, I. B.; Xiong, Y. Nonstructural Protein 1 of SARS-CoV-2 Is a Potent Pathogenicity Factor Redirecting Host Protein Synthesis Machinery toward Viral RNA. *Mol. Cell* **2020**, *80* (6), 1055−1066.

(14) Zhao, K.; Ke, Z.; Hu, H.; Liu, Y.; Li, A.; Hua, R.; Guo, F.; Xiao, J.; Zhang, Y.; Duan, L.; Yan, X.-F.; Gao, Y.-G.; Liu, B.; Xia, Y.; Li, Y. Structural Basis and Function of the N Terminus of SARS-CoV-2 Nonstructural Protein 1. *Microbiology Spectrum* **2021**, *9* (1), e00169−21.

(15) Tokuriki, N.; Oldfield, C. J.; Uversky, V. N.; Berezovsky, I. N.; Tawfik, D. S. Do viral proteins possess unique biophysical features? *Trends Biochem. Sci.* **2009**, *34* (2), 53−59.
(16) Martell, A. E.; Smith, R. M. *Critical Stability Constants*; Springer Science: 1989; Vol. *6*, p 643.
(17) Aronoff-Spencer, E.; Burns, C. S.; Avdievich, N. I.; Gerfen, G. J.; Peisach, J.; Antholine, W. E.; Ball, H. L.; Cohen, F. E.; Prusiner, S. B.; Millhauser, G. L. Identification of the Cu^{2+} Binding Sites in the N-Terminal Domain of the Prion Protein by EPR and CD Spectroscopy. *Biochemistry* **2000**, *39* (45), 13760−13771.
(18) Burns, C. S.; Aronoff-Spencer, E.; Dunham, C. M.; Lario, P.; Avdievich, N. I.; Antholine, W. E.; Olmstead, M. M.; Vrielink, A.; Gerfen, G. J.; Peisach, J.; Scott, W. G.; Millhauser, G. L. Molecular Features of the Copper Binding Sites in the Octarepeat Domain of the Prion Protein. *Biochemistry* **2002**, *41* (12), 3991−4001.
(19) Chattopadhyay, M.; Walter, E. D.; Newell, D. J.; Jackson, P. J.; Aronoff-Spencer, E.; Peisach, J.; Gerfen, G. J.; Bennett, B.; Antholine, W. E.; Millhauser, G. L. The Octarepeat Domain of the Prion Protein Binds Cu(II) with Three Distinct Coordination Modes at pH 7.4. *J. Am. Chem. Soc.* **2005**, *127* (36), 12647−12656.
(20) Manikandan, P.; Epel, B.; Goldfarb, D. Structure of Copper-(II)−Histidine Based Complexes in Frozen Aqueous Solutions As Determined from High-Field Pulsed Electron Nuclear Double Resonance. *Inorg. Chem.* **2001**, *40* (4), 781−787.
(21) Van Doorslaer, S.; Cereghetti, G. M.; Glockshuber, R.; Schweiger, A. Unraveling the Cu^{2+} Binding Sites in the C-Terminal Domain of the Murine Prion Protein: A Pulse EPR and ENDOR Study. *J. Phys. Chem. B* **2001**, *105* (8), 1631−1639.
(22) Stöckel, J.; Safar, J.; Wallace, A. C.; Cohen, F. E.; Prusiner, S. B. Prion Protein Selectively Binds Copper(II) Ions. *Biochemistry* **1998**, *37* (20), 7185−7193.
(23) Reed, J.; Reed, T. A. A Set of Constructed Type Spectra for the Practical Estimation of Peptide Secondary Structure from Circular Dichroism. *Anal. Biochem.* **1997**, *254* (1), 36−40.
(24) Pan, C.-P.; Muiño, P. L.; Barkley, M. D.; Callis, P. R. Correlation of Tryptophan Fluorescence Spectral Shifts and Lifetimes Arising Directly from Heterogeneous Environment. *J. Phys. Chem. B* **2011**, *115* (12), 3245−3253.
(25) Lee, J. C.; Gray, H. B.; Winkler, J. R. Copper(II) Binding to α-Synuclein, the Parkinson's Protein. *J. Am. Chem. Soc.* **2008**, *130* (22), 6898−6899.
(26) Lee, J. C.; Langen, R.; Hummel, P. A.; Gray, H. B.; Winkler, J. R. α-Synuclein structures from fluorescence energy-transfer kinetics: Implications for the role of the protein in Parkinson's disease. *Proc. Natl. Acad. Sci. U. S. A.* **2004**, *101*, 16466−16471.
(27) Förster, T. Zwischenmolekulare Energiewanderung und Fluoreszenz. *Ann. Phys. (Leipzig)* **1948**, *2* (6), 55−75.
(28) Winkler, J. R.; Gray, H. B. Long-Range Electron Tunneling. *J. Am. Chem. Soc.* **2014**, *136* (8), 2930−2939.
(29) Chang, I.-J.; Lee, J. C.; Winkler, J. R.; Gray, H. B. The Protein-Folding Speed Limit: Intrachain Diffusion Times Set by Electron-Transfer Rates in Denatured $Ru(NH_3)_5$(His-33)-Zn-cytochrome *c*. *Proc. Natl. Acad. Sci. U. S. A.* **2003**, *100* (7), 3838−3840.
(30) Hagen, S. J.; Hofrichter, J.; Eaton, W. A. Rate of Intrachain Diffusion of Unfolded Cytochrome *c*. *J. Phys. Chem. B* **1997**, *101*, 2352−2365.
(31) Szabo, A.; Schulten, K.; Schulten, Z. First Passage Time Approach to Diffusion Controlled Reactions. *J. Chem. Phys.* **1980**, *72* (8), 4350−4357.
(32) Thirumalai, D. Time Scales for the Formation of the Most Probable Tertiary Contacts in Proteins with Applications to Cytochrome *c*. *J. Phys. Chem. B* **1999**, *103* (4), 608−610.
(33) Peisach, J.; Blumberg, W. E. Structural implications derived from the analysis of electron paramagnetic resonance spectra of natural and artificial copper proteins. *Arch. Biochem. Biophys.* **1974**, *165* (2), 691−708.

https://doi.org/10.1021/acs.inorgchem.2c01329
Inorg. Chem. 2022, 61, 8992−8996